Applied Catalysis A, General 658 (2023) 119169

Contents lists available at ScienceDirect

Applied Catalysis A, General

journal homepage: www.elsevier.com/locate/apcata

Synergy between the proton conducting and a mixed electronic and oxygen ionic conducting phases in a composite anode for electrocatalytic propane ODH

Jaesung Kim [a], Dhruba J. Deka [a,1], Seval Gunduz [a], Anne C. Co [b], Umit S. Ozkan [a,*]

[a] William G. Lowrie Department of Chemical and Biomolecular Engineering, The Ohio State University, Columbus, OH 43210, United States
[b] Department of Chemistry and Biochemistry, The Ohio State University, Columbus, OH 43210, United States

ARTICLE INFO

Keywords:
Propane oxidative dehydrogenation
Electrocatalyst
Solid oxide cell
Perovskite
Proton conductive

ABSTRACT

Oxidative dehydrogenation (ODH) of propane offers an attractive and feasible method for increasing propylene production to meet the growing demand. In this study, a dual phase catalyst composed of proton conducting $SrCe_{0.95}Yb_{0.05}O_3$ (SCY) and mixed oxygen ionic and electronic conducting $(La_{0.8}Sr_{0.2})_{0.95}MnO_3$ (LSM) has been investigated for propane ODH. TPD-DRIFTS was used to study H_2O adsorption and the presence of basic lattice oxygen on the surface of SCY. The addition of 40 wt% SCY to LSM resulted in significant improvements in propane conversion and olefin selectivity. These enhancements were likely due to the highly basic nature of the SCY surface by helping rapid desorption of propylene resulting in high propylene yields. In addition, proton conductive SCY facilitated the proton abstraction from propane and its transport to the interface between SCY and LSM where an oxidation reaction occurs. It was demonstrated by TPrxn experiments using C_3H_8 and C_3H_6 that a moderate oxygen ionic conductivity and a basic surface of the catalyst are needed for the selective conversion of propane to olefins.

1. Introduction

Ethylene and propylene are the most widely used raw materials in the petrochemical industry [1]. Most of these olefins are produced through steam cracking of naphtha and heavy oils at high temperatures [2,3]. However, this conventional method is energy intensive and produces unwanted byproducts such as methane, hydrogen, NOx, and CO_x, leading to lower olefin selectivity. Furthermore, propylene is merely a byproduct of steam cracking, whereas ethylene is the main olefin product [3]. This imbalance between propylene supply and demand has spurred interest in propylene production.

One potential solution is the catalytic dehydrogenation (DH) of propane, which involves the removal of two hydrogen atoms from propane to produce propylene:

$$C_3H_8 \leftrightarrow C_3H_6 + H_2 \quad (1)$$

However, this reaction is endothermic and has thermodynamic limitations that restrict propane conversion [2,4]. An alternative approach is oxidative dehydrogenation (ODH), where the H_2 molecule formed during DH is removed by converting it to H_2O with an oxidant [2,4,5].

$$C_3H_8 + 0{\cdot}5\ O_2 \leftrightarrow C_3H_6 + H_2O \quad (2)$$

ODH is exothermic and requires lower operating temperatures compared to DH, which minimizes side reactions. Traditionally, ODH is performed in a fixed bed reactor with co-feeding of propane and oxygen. However, this can lead to lower propylene selectivity due to the reaction of propylene with gas phase oxygen to produce carbon oxides. To improve selectivity, researchers have explored alternative oxidants [6,7] and halide catalyst promoters [8–14], as well as new reactor designs with short contact times between reactants/products and the catalyst surface [15–17]. A solid oxide electrocatalytic cell (SOEC) offers the potential for improved selectivity by enabling the control of oxygen ion flux to the reaction medium via external current/voltage application [18].

Perovskite-type mixed metal oxides, with their ABO_3-type crystal structure, are mixed ionic-electronic conductors (MIECs) with excellent redox properties, tunable oxygen ion accessibility, high stability,

* Corresponding author.
E-mail address: Ozkan.1@osu.edu (U.S. Ozkan).
[1] Currently at Oak Ridge National Laboratory, Oak Ridge, Tennessee 37830, USA.

https://doi.org/10.1016/j.apcata.2023.119169
Received 16 December 2022; Received in revised form 11 March 2023; Accepted 27 March 2023
Available online 30 March 2023

resistance to coke formation, and easily tunable surface properties such as acidity/basicity [19–24]. ODH of alkanes on perovskite oxides follows the Mars van Krevelen (MvK) reaction mechanism, which involves C–H bond activation with lattice oxygen [22].

High-temperature solid state proton conductors have been studied since the discovery of proton conductivity in barium and strontium cerate-based materials in the 1980′s [25]. Materials based on $BaZrO_3$, $BaCeO_3$, $SrZrO_3$ and $SrCeO_3$ have now been widely accepted as high-temperature proton conductors [26–30]. When an alkane adsorbs on the surface of these materials, a hydrogen atom can potentially be abstracted by an adjacent lattice oxygen to form an OH^- ion. The proton can then migrate through the oxide ions, giving the perovskite protonic conductivity.

In this study, a dual phase composite material composed of a cerate proton conductor with the formula $SrCe_{0.95}Yb_{0.05}O_3$ (SCY) and mixed electronic and oxygen ionic conductor (MIEC) $(La_{0.8}Sr_{0.2})_{0.95}MnO_3$ (LSM) was investigated as an anode catalyst for electrocatalytic propane ODH. A schematic illustration of the process can be found in Fig. 1. The presence of basic lattice oxygen on the surface of SCY was found to be crucial for the selective conversion of propane to olefins. Moreover, the dual phase catalyst effectively improved propane ODH by facilitating the abstraction of protons and their transfer to the interface between SCY and LSM.

2. Experiments

2.1. Preparation of catalysts

Citric acid-ethylenediaminetetraacetic acid (EDTA) complexation method was used to prepare $SrCe_{0.95}Yb_{0.05}O_3$ (SCY). Stoichiometric amounts of strontium carbonate ($Sr(CO_3)_2$), cerium nitrate hexahydrate ($Ce(NO_3)$•6 H_2O) were dissolved in 100 ml of deionized water. EDTA and citric acid at 1:1 ratio to the total metal ions were added to the solution at room temperature. At 60 °C, ammonium hydroxide was added to the solution to stabilize the pH at 6. The solution was heated to 80 °C, maintaining a pH of 6. Afterward, the gel formed was dried at 150 °C. Crystalline SCY was obtained by calcining the dried powders for 2 h at 1000 °C. $(La_{0.8}Sr_{0.2})_{0.95}MnO_3$ was purchased from Nextech Materials. LSM and SCY were mixed at different weight ratios ($(LSM)_x(SCY)_{(10-x)}$, (x = 0,2,4,6,8)).

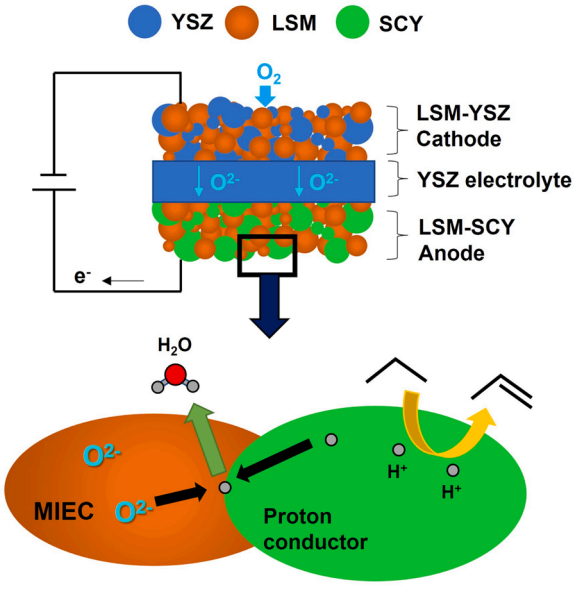

Fig. 1. Schematic illustration of electrocatalytic propane ODH on the dual phase anode catalyst consisting of LSM and SCY.

2.2. Evaluation of electrocatalytic performance

A button cell was fabricated using a screen-printing technique on a commercial yttria-stabilized zirconia (YSZ) electrolyte (25 mm in diameter, 125 μm in thickness; Nextech Materials). A slurry mixture of SCY and LSM at different weight ratios was screen-printed on the anode side. LSM-YSZ was also screen-printed onto the cathode side and then fired at 1200 °C for 2 h. Gold paste was used to attach the current collectors (silver wires) on both electrodes. 5ccm of 10 % C_3H_8/He was flowed into the anode chamber and cathode side was open to air. The electrochemical impedance spectrum (EIS) was collected with frequencies ranging from 1 MHz to 10 mHz using a potentiostat (BioLogic). The gas products were quantified using a pulse discharge helium ionization detector (PDHID) and a flame ionization detector (FID) in an online gas chromatograph (Shimadzu 2014).

2.3. Material characterization

Bruker D8 Lead X-ray powder diffractometer equipped with Cu Kα X-ray source was used to measure the X-ray diffraction patterns. The voltage and current in the generator were 40 kV and 40 mA, respectively. The 2θ scan range was 20–60° and the step size was 0.014° per 0.5 s

An MKS Cirrus mass spectrometer was used to analyze the effluent produced during the temperature-programmed experiments under 30ccm of 5 % H_2/N_2, 1 % H_2O/He, 10 % C_3H_8/He, or 10 % C_3H_6/He. These experiments were conducted by packing catalyst powders into a quartz reactor and heated with a ramp rate of 10 °C min^{-1}. All the samples were pretreated with 10 % O_2/He up to 1000 °C before temperature-programmed experiment.

Thermoelectron Nicolet 6700 FTIR equipped with an MCT detector was used to collect temperature-programmed desorption (TPD) -diffuse reflectance infrared Fourier transform spectroscopy (DRIFTS) data. Helium pretreatment of the samples at 450 °C was performed to desorb any surface adsorbed species. The background spectra were acquired during a cooling process from 450 °C to 50 °C, following the pretreatment. DRIFTS spectra were collected during a heating process under helium after exposing the samples to H_2O or CO_2 at 50 °C. The DRIFTS spectra were plotted by subtracting the background spectra from probe molecules absorbed spectra at the corresponding temperatures.

X-ray Absorption Near Edge Spectroscopy (XANES) was performed on the catalyst powders at Sector 10-BM of the Materials Research Collaborative Access Team (MRCAT) at the Advanced Photon Source (APS, Argonne National Laboratory). Athena software was used to process the collected data [31].

Electrical conductivity of catalyst samples was carried out on pellets formed by compressing the powder in a hydraulic press, followed by sintering at 1300 °C for 5 h. Four gold wires were connected to four points on the pellet using gold paste. A Keithley 6220 current source was connected to the two leads for current application and Keithley 6182 sensitive nanovoltmeter was connected to the other two leads to measure the corresponding voltages.

3. Results and discussions

3.1. Structural analysis

The crystalline structure of SCY and LSM was studied using X-ray diffraction (XRD) technique. Fig. 2 shows XRD patterns of the powder materials before and after the thermochemical treatment with 5 % H_2/N_2 at 850 °C for 2 h. The as-prepared LSM powder had a rhombohedral perovskite crystal structure with no impurities [32]. The XRD pattern of SCY showed a distorted orthorhombic perovskite structure with a space group Pbnm, which transformed to cubic symmetry when heated to 850 °C [33]. Both perovskite materials showed an excellent thermochemical stability, with intact XRD patterns, although SCY showed a

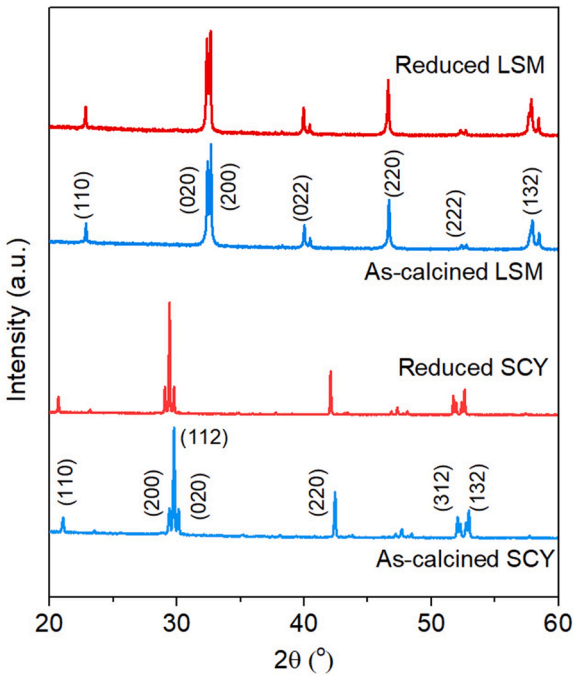

Fig. 2. XRD patterns of SCY and LSM before and after reduction.

slight shift towards lower 2θ values, possibly due to unit cell expansion.

Temperature-programmed reduction (TPR) was conducted under 30ccm of 5 % H_2/N_2 by monitoring H_2O signal ($m/z = 18$). In Fig. 3, LSM showed two distinct peaks, while SCY did not have a noticeable peak. The first peak on the TPR curve of LSM is attributed to the reduction of Mn^{4+} to Mn^{3+} and the formation of oxygen vacancies, and the second peak to the reduction of Mn^{3+} to Mn^{2+} [34]. The TPR results of SCY are in alignment with literature, which suggested that only a minimal proportion, approximately 1 %, of cerium ions undergo reduction to the trivalent state [35]. The high reducibility of LSM suggests that it has a higher oxide ion conductivity, potentially leading to complete oxidation of propane or propylene to CO_x.

3.2. TPD-DRIFTS analysis

An analysis of the acidic/basic surface characteristics of the SCY and LSM was performed using TPD-DRIFTS. CO_2 is known as a probe molecule for the basic sites on metal oxides. In metal oxides, Lewis basic sites are commonly found as basic hydroxyl groups or surface lattice oxygens. The interaction of CO_2 with basic OH groups or surface oxygen groups may lead to the formation of bicarbonates and other carbonates, respectively. In Fig. 4(a), on the SCY surface, CO_2 adsorption led to the formation of various surface species, including bicarbonates (1610 cm^{-1} and 1212 cm^{-1}) and carbonates (1025–1060 cm^{-1}, 1295 cm^{-1}, 1575 cm^{-1}, and 1672 cm^{-1}) [36,37]. On the SCY surface, both bicarbonate and carbonate vibrations suggest that both OH^- and lattice oxygen sites are present, and the persistence of the corresponding bands even at elevated temperatures indicates a strong basicity. It has been found that an increase in surface basicity leads to an enhancement in the desorption of alkenes, resulting in improved selectivity [38,39]. Therefore, the presence of basic lattice oxygen on the surface of SCY as shown by TPD-DRIFTS of CO_2 suggests SCY as a potential catalyst for propane ODH. However, the bicarbonate and carbonate bands were absent on the spectra for LSM, which indicates extremely weak basicity of the LSM surface (Fig. S1(a)).

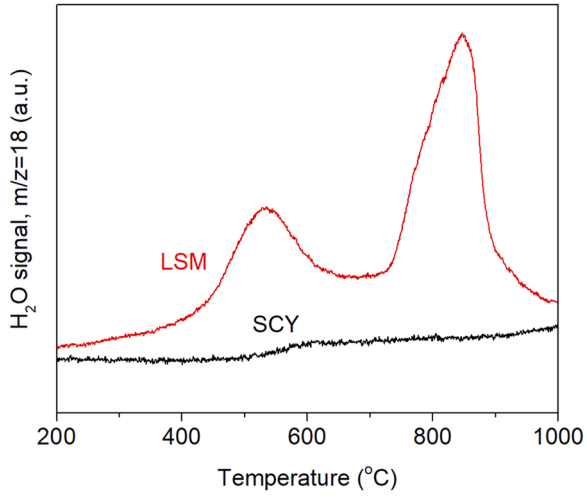

Fig. 3. TPR profiles of SCY and LSM under 30 ccm of 5 % H_2/N_2 at a ramp rate of 10 °C min^{-1}.

Water adsorption and hydroxyl group formation are crucial characteristics for proton conductive materials since hydroxyl ions provide the "hopping" sites for protons [33]. For water to dissociate, oxygen vacancies are necessary as indicated by the following Kröger-Vink's equation:

$$H_2O + V_O^{\bullet\bullet} + O_O^X \leftrightarrow 2OH^{\bullet} \quad (3)$$

TPD-DRIFTS were used to investigate the adsorption of water on the surface of SCY. The broad band between 3000 cm^{-1} and 3700 cm^{-1} is corresponding to the stretch modes of hydrogen-bonded –OH in Fig. 4 (b). The broad nature of the band results from hydrogen bonds between water molecules. The sharp peak at 1630 cm^{-1} is attributed to H_2O bending vibration of residual adsorbed water [40,41]. When hydrogen bonds are formed, water molecules vibrate at a frequency higher than that of freely rotating water, which has a 1595 cm^{-1} frequency. Considering the peak found at 1630 cm^{-1}, water molecules are likely to form dimeric or polymeric hydrogen bonds on the SCY surface. However, no such peak was seen on the surface of LSM in Fig. S1(b).

H_2O adsorption was also investigated using mass spectroscopy by monitoring H_2O signal ($m/z = 18$) while heating SCY and LSM powders under He. Fig. 5(a) shows the H_2O desorption profiles on SCY and LSM powders treated with H_2O at room temperature. The desorption of water molecules began at around 100 °C on both samples, but the amount of water desorbed on SCY was much greater than that on LSM. This desorption may be attributed to the water molecules physically adsorbed on the surface of the catalysts. A further water desorption peak was observed only on SCY at temperatures above 400 °C. It can be hypothesized that the water molecules have chemically bonded to the SCY since the desorption temperature is greater than 400 °C. Moreover, it is likely that the desorbed water above 400 °C originated from the perovskite lattice as $OH^{\bullet}$ in Eq. 3, considering the massive amount of evolution. Fig. 5(b) shows the result of further investigation under continuous 1 % H_2O/He flow through the SCY and LSM catalyst beds at elevated temperatures. H_2O adsorption was performed at 400 °C until the H_2O signal is stabilized to saturate the samples and then, the samples were heated up to 600 °C. When the temperature was increased, H_2O signal increased only on SCY. Since the starting temperature was at 400 °C, the adsorbed amount of water on the catalysts surface would be minimal. Therefore, the increased H_2O signal upon increasing temperature is likely due to the water molecules being evolved from the perovskite lattice, indicative of the high proton conductivity of SCY. It is expected that the proton conductive nature of the SCY would assist in transporting hydrogen atoms that have been abstracted from propane to the interface between the SCY and the LSM, where the oxidation reaction occurs, resulting in the production of water.

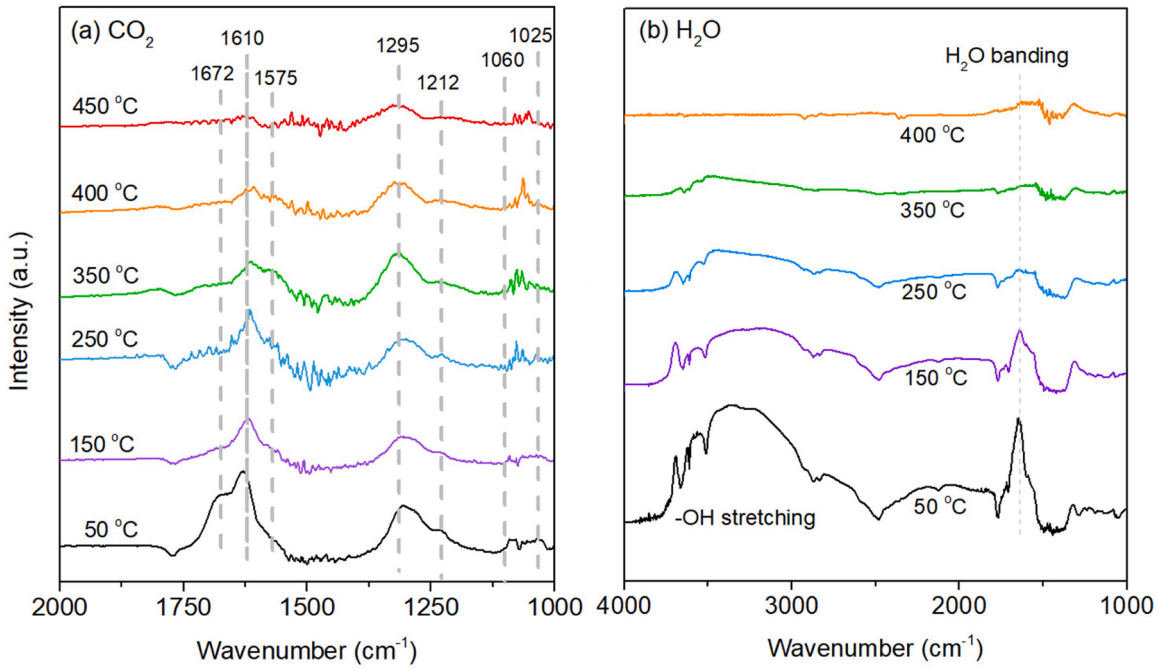

Fig. 4. TPD-DRIFTS of CO_2 and H_2O on SCY.

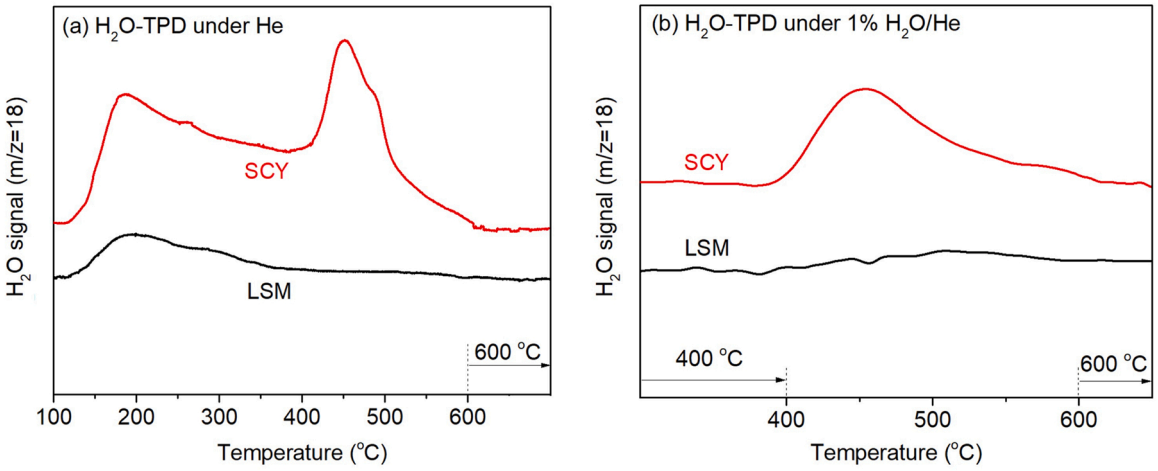

Fig. 5. (a) TPD of H_2O under He, (b) evolution of H_2O on heating from 400 °C to 600 °C under 1 % H_2O/He flow.

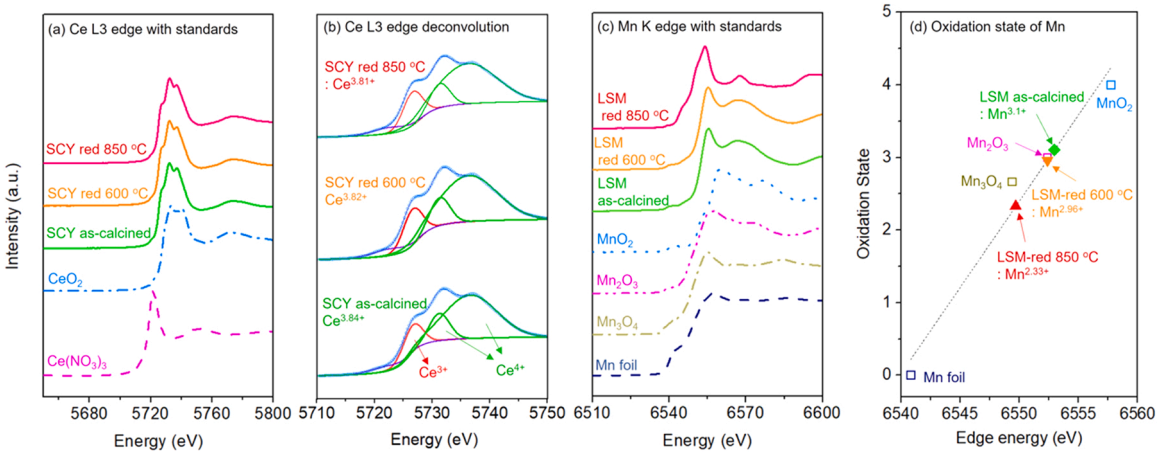

Fig. 6. (a) XANES spectra of Ce L3 edge and (b) deconvoluted spectra, (c) XANES spectra of Mn K edge and (d) approximated oxidation state of Mn.

3.3. Investigation of elemental oxidation state

Fig. 6 shows the normalized Ce L3 edge XANES spectra of SCY and Mn K edge of LSM along with the standard compounds. The edge energy of Ce L3 edge of as-calcined SCY powders was measured as 5725.5 eV in Fig. 6(a), which was between Ce^{3+} (5719.6 eV) on $Ce(NO_3)_3$ and Ce^{4+} (5728.0 eV) on CeO_2. The Ce L3 edge energy of SCY reduced at 600 °C under 5 % H_2/N_2 for 2 h (SCY red 600 °C) was 5725.4 eV. It shifted to a lower energy, 5725.2 eV, after the reduction at 850 °C (SCY red 850 °C). The XANES spectra of Ce L3 edge of SCY samples were deconvoluted as shown in Fig. 6(b). The estimated oxidation states of Ce ions in SCY perovskites decrease from 3.84 to 3.82 and to 3.81 following the reduction at 600 °C and 850 °C, respectively. The lower than expected oxidation state of Ce (4 +) in the as-synthesized SCY suggests the presence of oxygen vacancies, which may be caused by the addition of doped Yb ions [42]. In view of such minimal changes in the oxidate state, SCY is considered to have moderate oxygen accessibility, which prevents complete oxidation of propane or propylene to CO_x.

The Mn K edge energy of as-calcined LSM was found as 6552.97 eV which is very close to that of Mn_2O_3, 6553.0 eV. The edge energy slightly decreased to 6552.4 eV after reduction at 600 °C (LSM red 600 °C). It further shifted to 6549.7 eV after the reduction at 850 °C (LSM red 850 °C). The oxidation state of Mn ions estimated by a linear fitting decreased from 3.1 to 2.33 as shown in Fig. 6(d). Since the redox behavior of B-site ions is related to catalytic activity, LSM perovskites have high oxygen accessibility, resulting in complete oxidation of propane and propylene to CO_x [43].

3.4. Electrical conductivity

Electrical conductivity was measured using the four-probe van der Pauw method at a temperature range of 25 °C–600 °C for LSM and mixtures of LSM and SCY as shown in Fig. 7(a). LSM has a high conductivity, ranging between 39 S cm^{-1} and 153 S cm^{-1} in the measured temperature range. SCY, on the other hand, is an electrically insulating material. It is therefore necessary to mix it with electrically conductive LSM to serve as an electrode. Increasing amounts of LSM were found to result in increased conductivity for the SCY and LSM composite mixtures. The electrical conductivity of $(LSM)_6(SCY)_4$ was measured to be 10.3 S cm^{-1} at 600 °C, which is above the generally acceptable level of conductivity of 10 S cm^{-1} for densified electrode materials in SOEC/SOFC applications [44]. The electrical conductivity followed a linear Arrhenius relationship over the entire temperature range (Fig. 7(b)), indicating that LSM and the mixtures of LSM and SCY follow a small polaron conduction mechanism [45]. An activation energy of 0.12 eV was measured for LSM, which is consistent with literature [45]. The activation energy of the electrical conductivity of the LSM and SCY composite increased from 0.11 to 0.25 eV with increasing contents of SCY.

3.5. Electrocatalytic performance for propane ODH

The electrocatalytic performance of dual phase LSM and SCY catalyst anodes was investigated for propane ODH with 5 ccm of 10 % C_3H_8/He at 600 °C. The SEM images of LSM and $(LSM)_6(SCY)_4$ after densification at 1200 °C are presented in Fig. S2. The $(LSM)_6(SCY)_4$ exhibits smaller particles size compared to LSM, which may be due to the higher temperature requirement for densification of SCY. Both electrodes were densified to an adequate level, ensuring good mixed ionic and electric conductivity. The electrocatalytic propane conversion and propylene selectivity were obtained under 10 mA of applied current on the dual phase catalysts at different ratios. SCY could not be evaluated as an electrode material because it does not have adequate electrical conductivity. Propane conversion under open-circuit voltage (OCV) was 6.7 % on LSM but less than 3 % for the LSM-SCY composite catalysts at 600 °C. This is because propane is readily activated by oxygen and LSM has high oxygen ionic conductivity, which facilitates oxygen transport to the anode surface even under OCV. To assess the effect of electrocatalysis, the electrocatalytic conversion of propane was calculated as the propane conversion under closed-circuit subtracted by the propane conversion under OCV.

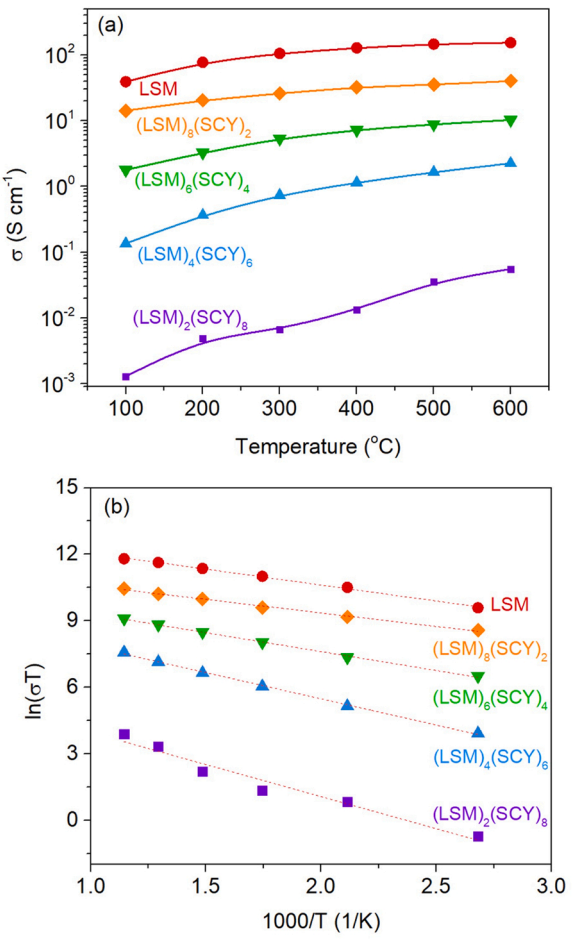

Fig. 7. Electrical conductivity measurement on the mixtures of LSM and SCY at different weight ratios.

The electrocatalytic propane conversion is shown as red circles in Fig. 8 increased from 3.5 % on LSM to 8.1 % on $(LSM)_2(SCY)_8$. This is likely due to the ability of SCY to activate propane and facilitate the

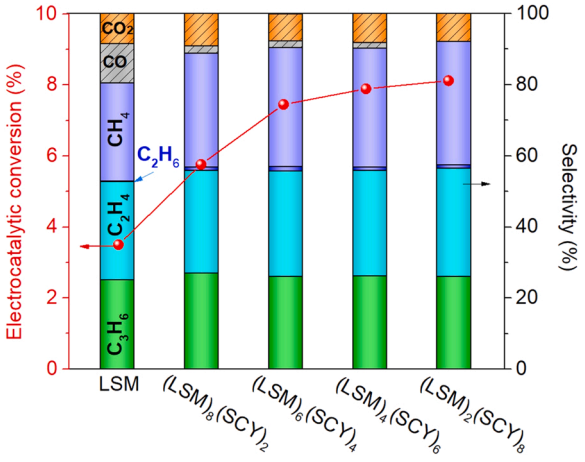

Fig. 8. Electrocatalytic performance for propane ODH on the dual phase LSM and SCY catalyst anodes at different weight ratios under 10 mA at 600 °C.

hydrogen atom abstraction [46]. Specifically, a proton is abstracted from propane molecule, leaving a propyl anion on the SCY surface. Then, a hydride ion is removed from the propyl anion releasing propylene. When two electrons are removed from the hydride ion, a proton is formed. Since this is an electrocatalytic reaction, it is expected that a higher current density would lead to higher propane conversion. In addition, the electrochemical environment on the anode promotes the oxidation of the hydride ions to protons, hence preventing them from being released to the reaction environment as H_2. This, in turn, suppresses the reverse of the non-oxidative dehydrogenation (i.e., hydrogenation reaction). This may also contribute to the increased propane conversion with increasing current densities. Increasing SCY ratios led to a substantial decrease in CO_x selectivity, from 19.5 % to 7.9 %, as well as an increase in olefin selectivity including propylene and ethylene, with a combined selectivity from 52.7 % to 55.8 %. The high basicity of the SCY surface may explain the enhanced olefin selectivity and lowered CO_x selectivity. When propane adsorbs on the surface of SCY, C–H bond activation and hydrogen abstraction take place, producing propylene. Propylene adsorbed on the basic SCY surface can readily desorb, leading to high propylene selectivity. The proton conductivity of SCY can also contribute to decreasing the rehydrogenation reaction rate, as the H-atom abstracted from propane is transported to the interface between SCY and LSM, where oxidation reaction takes place to produce water.

In Fig. 9, the electrocatalytic performances of $(LSM)_6(SCY)_4$ and LSM were compared under different applied currents at 600 °C. With the increase in applied current from 5 mA to 20 mA, the propane conversion increased about 3 times from 3.7 % to 11.3 % on $(LSM)_6(SCY)_4$, while the increase was about 2 times on LSM from 3.5 % to 7.2 %. The selectivity did not change much with increased current, however, higher currents resulted in greater olefin yields on $(LSM)_6(SCY)_4$ compared to those on LSM as shown in Fig. 9(c). The fact that product selectivity remains unchanged, while the propane conversion increases with increasing current, suggests that the first dehydrogenation of propane is electrocatalytically initiated, while subsequent steps, such as desorption of propylene gas or cracking to ethylene and methane, are independent of the electrochemical process. As a result, the increase of carbon oxides selectivity was not significant with the increase in current. This differs from ODH in thermal catalysis where the rate was reported to be independent of oxygen partial pressure. Also, in thermal catalysis, olefin selectivity always decreases with increasing conversion. The fact that the selectivity remained essentially constant with increasing conversion in this study signals different mechanisms being in operation in electrocatalysis and thermal catalysis ODH reactions [47].

The cell voltage of $(LSM)_6(SCY)_4$ and LSM electrodes were measured for 3 h under during electrocatalytic propane ODH reaction at 600 °C (Fig. 10(a,b)). The cell voltage of $(LSM)_6(SCY)_4$ ranged between 0.68 V and 1.33 V for propane ODH and appeared to be stable for 3 h. On the other hand, the cell voltage of LSM anode was not stable and exhibited an increase for the three applied current values. Specifically, the cell voltage increased from 0.61 V to 0.74 V at 20 mA. Electrochemical impedance spectra (EIS) were obtained on $(LSM)_6(SCY)_4$ and LSM for propane ODH (Fig. 10(c,d)). The ohmic resistance at the X-axis intercept at high frequency, was measured as 15 Ω cm^2 on $(LSM)_6(SCY)_4$, which was higher than that on LSM, at 11 Ω cm^2. Given that ohmic resistance is attributed to electrolyte, current collector, and contact resistance between electrode and current collector, the higher resistance on $(LSM)_6(SCY)_4$ is likely due to the contact resistance between $(LSM)_6(SCY)_4$ and current collector [48]. $(LSM)_6(SCY)_4$ has 40 wt% electrically insulting SCY, which may result in an increase in contact resistance between the electrode and the current collector. $(LSM)_6(SCY)_4$ also had a higher polarization resistance than LSM because of its lower electrical conductivity. However, on $(LSM)_6(SCY)_4$, polarization resistance decreased significantly with increasing applied current, which indicates propane ODH is electrocatalytically activated. On the other hand, the polarization resistance on LSM remained almost the same as the current increased.

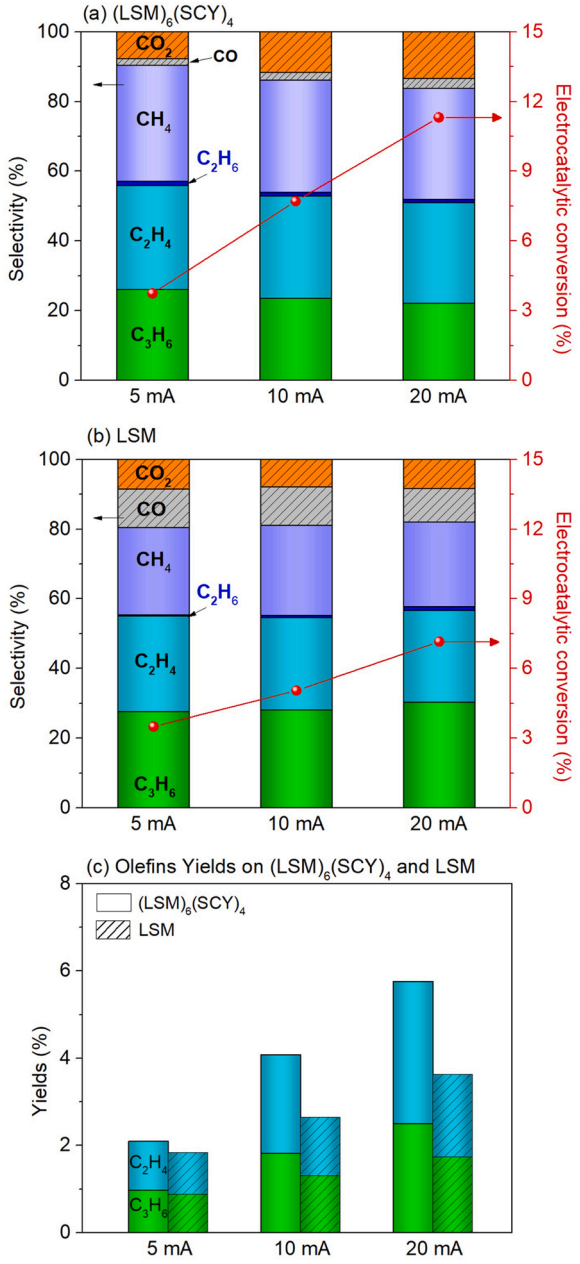

Fig. 9. Electrocatalytic performance for propane ODH on (a) $(LSM)_6(SCY)_4$ and (b) LSM under different currents, and (c) corresponding olefins yields.

3.6. *Temperature-programmed reactions*

The activation of propane and propylene on SCY and LSM catalysts was investigated using the temperature-programmed reaction (TPrxn) technique. Fig. 11 shows the evolution of main products such as propylene, CO, and CO_2 throughout the TPrxn process. It should be noted that lattice oxygen in the structure of SCY and LSM perovskite oxides was the only oxygen source used in this set of experiments. Compared to SCY, peaks corresponding to CO and CO_2 were much larger on LSM, showing that propane is oxidized to CO_x more readily on LSM. The ratios of propylene-to-CO_x were calculated based on the area under the curves for the two electrocatalytic materials. The propylene-to-CO_x ratio on SCY was 2.0 which was much higher than 0.3 on LSM, indicating higher propylene selectivity of SCY over CO_x. Moreover, TPrxn under propylene was conducted on SCY and LSM by monitoring CO_2 signal ($m/z = 44$) in Fig. 11(c). An intense CO_2 peak was observed on LSM catalyst

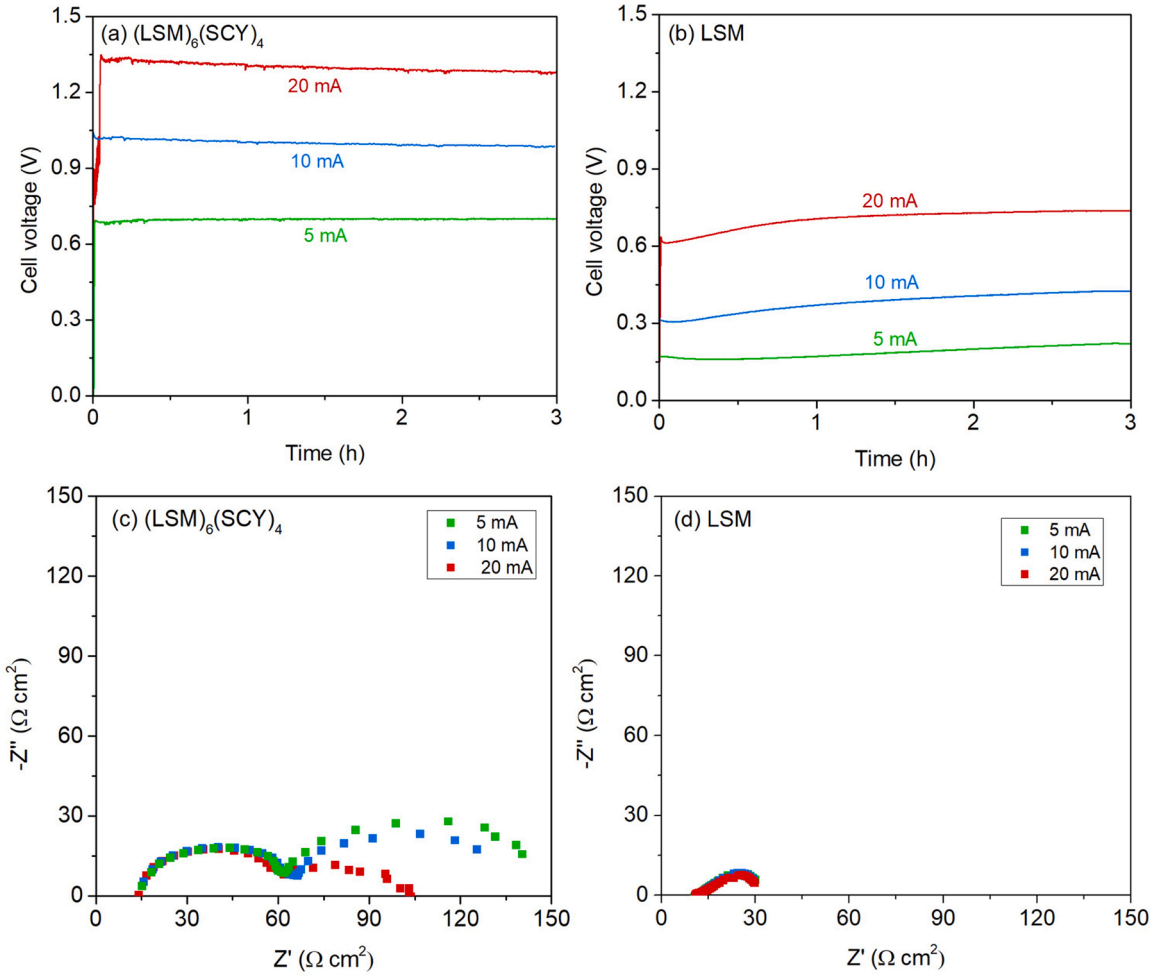

Fig. 10. Cell voltage for the electrocatalytic propane ODH for 3 h on (a) $(LSM)_6(SCY)_4$ and (b) LSM at 600 °C. Electrochemical impedance spectra for propane ODH on (c) $(LSM)_6(SCY)_4$ and (d) LSM.

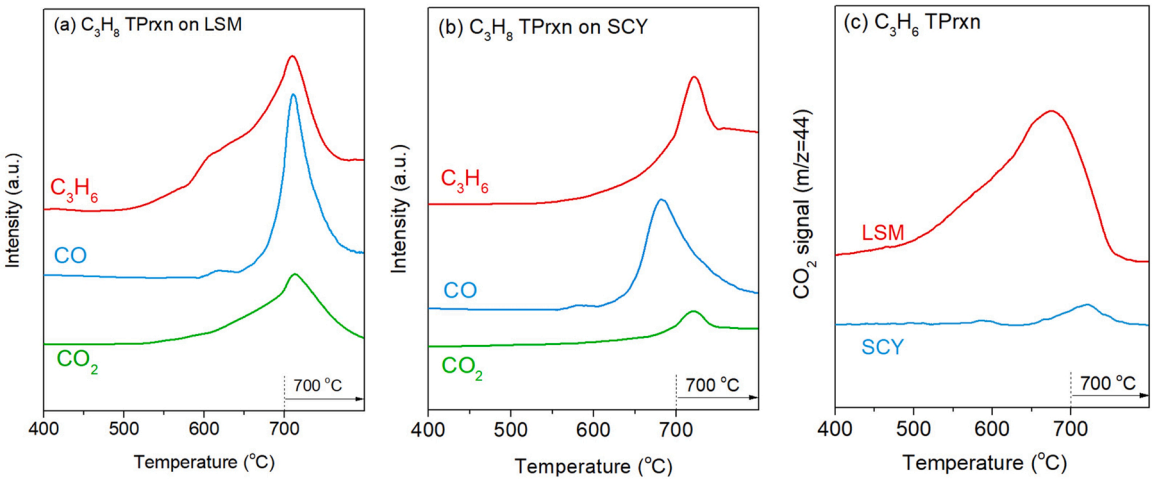

Fig. 11. TPrxn on (a) LSM and (b) SCY under 10 % C_3H_8/He by collecting C_3H_6, CO, and CO_2 signals, (c) TPrxn on LSM and SCY under 10 % C_3H_6/He by monitoring CO_2 signal.

starting 400 °C while a minimal peak was detected on SCY at 700 °C. It is due to the highly basic surface of SCY that provides a fast desorption of propylene before further oxidation to CO_x as well as the moderate oxygen mobility of SCY. Therefore, for better propylene selectivity, the catalytic/electrocatalytic material should have a moderate oxygen accessibility to prevent complete combustion of propylene, and high proton accessibility to selectively activate propane in favor of propylene.

4. Conclusions

A dual phase catalyst consisting of proton conductive SCY and mixed oxygen ionic and electronic conductive LSM was investigated for its ability to improve electrocatalytic propane ODH. When 40 wt% of SCY was mixed with LSM, the electrocatalytic performance for propane ODH improved the electrocatalytic conversion of propane and olefin yields. This performance improvement was attributed to the highly basic nature of the SCY surface which facilitated the rapid desorption of propylene and resulted in high propylene yields. In addition, the proton conductive SCY helped the hydrogen abstraction step as well as the transport of abstracted hydrogen to the interface between SCY and LSM where an oxidation reaction occurs. TPrxn experiments with C_3H_8 and C_3H_6 showed that SCY barely activated propylene while LSM oxidized both propane and propylene to CO_x, indicating that a moderate oxygen ionic conductivity and a basic surface of the catalyst are necessary for the selective conversion of propane to olefins.

CRediT authorship contribution statement

Jaesung Kim: Conceptualization, Investigation, Methodology, Data curation, Formal analysis, Writing – original draft. **Dhruba Jyoti Deka:** Conceptualization, Investigation, Methodology, Formal analysis, Writing – review & editing. **Seval Gunduz:** Investigation, Formal analysis, Writing – review & editing. **Anne C. Co:** Formal analysis, writing & review. **Umit S. Ozkan:** Conceptualization, Funding acquisition, Project administration, Resources, Supervision, Formal analysis, Writing – review & editing.

Declaration of Competing Interest

The authors declare that they have no known competing financial interests or personal relationships that could have appeared to influence the work reported in this paper.

Data availability

Data will be made available on request.

Acknowledgement

We would like to gratefully acknowledge the financial support provided for this work by the U.S. Department of Energy, Office of Science, Office of Basic Energy Sciences under the Award Number DE-FG02-07ER15896 and the U.S. National Science Foundation, under the award number 1932638. This research used resources of the Advanced Photon Source, a U.S. Department of Energy (DOE) Office of Science User Facility operated for the DOE Office of Science by Argonne National Laboratory under Contract No. DE-AC02-06CH11357.

Appendix A. Supporting information

Supplementary data associated with this article can be found in the online version at doi:10.1016/j.apcata.2023.119169.

References

[1] N. Sridhar, D. Hill, A. Agarwal, Y. Zhai, E. Hektor, Carbon Dioxide Utilization. Electrochemical Conversion of CO2–Opportunities and Challenges, Research and Innovation, Position Paper, 7 (2011).
[2] M.M. Bhasin, Is true ethane oxydehydrogenation feasible? Top. Catal. 23 (2003) 1–4.
[3] J.S. Plotkin, The Propylene Gap: How Can It Be Filled?, Industrial Chemistry and Engineering, (2015).
[4] M.M. Bhasin, J.H. McCaina, B.V. Vora, T. Imai, P.R. Pujado, Dehydrogenation and oxydehydrogenation of paraffins to olefins, Appl. Catal. A Gen. 221 (2001) 397–419.
[5] H.H. Kung, Oxidative dehydrogenation of light (C2 to C4) alkanes, advances oin, Catalysis 40 (1994) 1–38.
[6] M.P. Woods, B. Mirkelamoglu, U.S. Ozkan, Oxygen and nitrous oxide as oxidants: implications for ethane oxidative dehydrogenation over silica− titania-supported molybdenum, J. Phys. Chem. C 113 (2009) 10112–10119.
[7] N. Mimura, I. Takahara, M. Inaba, M. Okamoto, K. Murata, High-performance Cr/H-ZSM-5 catalysts for oxidative dehydrogenation of ethane to ethylene with CO_2 as an oxidant, Catal. Commun. 3 (2002) 257–262.
[8] R.B. Watson, S.L. Lashbrook, U.S. Ozkan, Chlorine modification of Mo/silica-titania mixed-oxide catalysts for the oxidative dehydrogenation of ethane, J. Mol. Catal. A Chem. 208 (2004) 233–244.
[9] C. Liu, R.B. Watson, U.S. Ozkan, Spectroscopic characterization of Cl-modified Mo/Si: Ti catalysts for oxidative dehydrogenation of propane, Top. Catal. 41 (2006) 63–72.
[10] C. Liu, U.S. Ozkan, Spectroscopic and structural characterization of chlorine loading effects on Mo/Si: Ti catalysts in oxidative dehydrogenation of ethane, J. Phys. Chem. A 109 (2005) 1260–1268.
[11] U.S. Ozkan, R.B. Watson, The structure–function relationships in selective oxidation reactions over metal oxides, Catal. Today 100 (2005) 101–114.
[12] C. Liu, U.S. Ozkan, Effect of chlorine on redox and adsorption characteristics of Mo/Si: Ti catalysts in the oxidative dehydrogenation of ethane, J. Mol. Catal. A Chem. 220 (2004) 53–65.
[13] S.J. Conway, J.H. Lunsford, The oxidative dehydrogenation of ethane over chlorine-promoted lithium-magnesium oxide catalysts, J. Catal. 131 (1991) 513–522.
[14] S. Sugiyama, K. Sogabe, T. Miyamoto, H. Hayashi, J.B. Moffat, Oxidative dehydrogenation of ethane on rare earth oxides: effects of chlorine additives in gas and solid phase on the oxidation over cerium oxide, Catal. Lett. 42 (1996) 127–133.
[15] A. Beretta, E. Ranzi, P. Forzatti, Oxidative dehydrogenation of light paraffins in novel short contact time reactors. Experimental and theoretical investigation, Chem. Eng. Sci. 56 (2001) 779–787.
[16] D.K. Zerkle, M.D. Allendorf, M. Wolf, O. Deutschmann, Understanding homogeneous and heterogeneous contributions to the platinum-catalyzed partial oxidation of ethane in a short-contact-time reactor, J. Catal. 196 (2000) 18–39.
[17] B. Silberova, M. Fathi, A. Holmen, Oxidative dehydrogenation of ethane and propane at short contact time, Appl. Catal. A Gen. 276 (2004) 17–28.
[18] S. Gunduz, D. Dogu, D.J. Deka, K.E. Meyer, A. Fuller, A.C. Co, U.S. Ozkan, Application of solid electrolyte cells in ion pump and electrolyzer modes to promote catalytic reactions: an overview, Catal. Today 323 (2019) 3–13.
[19] R.R. Hudgins, P.L. Silveston, C.-Y. Li, A.A. Adesina. Partial Oxidation and Dehydrogenation of Hydrocarbons, Periodic Operation of Chemical Reactors, Elsevier, 2013, pp. 79–122.
[20] R. Watanabe, Y. Hondo, K. Mukawa, C. Fukuhara, E. Kikuchi, Y. Sekine, Stable and selective perovskite catalyst for dehydrogenation of propane working with redox mechanism, J. Mol. Catal. A Chem. 377 (2013) 74–84.
[21] S. Royer, D. Duprez, F. Can, X. Courtois, C. Batiot-Dupeyrat, S. Laassiri, H. Alamdari, Perovskites as substitutes of noble metals for heterogeneous catalysis: dream or reality, Chem. Rev. 114 (2014) 10292–10368.
[22] K. Chen, E. Iglesia, A.T. Bell, Isotopic tracer studies of reaction pathways for propane oxidative dehydrogenation on molybdenum oxide catalysts, J. Phys. Chem. B 105 (2001) 646–653.
[23] S. Cimino, F. Donsì, G. Russo, D. Sanfilippo, Optimization of ethylene production via catalytic partial oxidation of ethane on Pt–$LaMnO_3$ catalyst, Catal. Lett. 122 (2008) 228–237.
[24] F. Donsì, S. Cimino, R. Pirone, G. Russo, D. Sanfilippo, Crossing the breakthrough line of ethylene production by short contact time catalytic partial oxidation, Catal. Today 106 (2005) 72–76.
[25] H. Iwahara, T. Esaka, H. Uchida, N. Maeda, Proton conduction in sintered oxides and its application to steam electrolysis for hydrogen production, Solid State Ion. 3–4 (1981) 359–363.
[26] R. Hancke, Z. Li, R. Haugsrud, Hydrogen surface exchange on proton conducting oxides studied by gas phase analysis with mass spectrometry, J. Membr. Sci. 439 (2013) 68–77.
[27] K.D. Kreuer, Proton-conducting oxides, Annu. Rev. Mater. Res. 33 (2003) 333–359.
[28] L. Malavasi, C.A. Fisher, M.S. Islam, Oxide-ion and proton conducting electrolyte materials for clean energy applications: structural and mechanistic features, Chem. Soc. Rev. 39 (2010) 4370–4387.
[29] F. Su, C. Xia, R. Peng, Novel fluoride-doped barium cerate applied as stable electrolyte in proton conducting solid oxide fuel cells, J. Eur. Ceram. Soc. 35 (2015) 3553–3558.
[30] M. Swift, C.G. Van, de Walle, Impact of point defects on proton conduction in strontium cerate, J. Phys. Chem. C 120 (2016) 9562–9568.
[31] B. Ravel, N. M, ATHENA, ARTEMIS, HEPHAESTUS: data analysis for X-ray absorption spectroscopy using IFEFFIT, J. Synchrotron Radiat. (2005) 537–541.
[32] V. Sedykh, V.S. Shekhtman, I.I. Zverkova, A.V. Dubovitskii, V.I. Kulakov, Reversibility of structure phase transitions in $LaMnO_{3+\delta}$ manganite under heat treatment, Phys. C Supercond. 433 (2006) 189–194.
[33] K.S. Knight, Structural and thermoelastic study of the protonic conducting perovskite $SrCe_{0.95}Yb_{0.05}O_{\xi}$ ($\xi \sim 3$) between 373 K and 1273 K, J. Electroceram. 27 (2011) 143–153.
[34] J. Zhu, H. Li, L. Zhong, P. Xiao, X. Xu, X. Yang, Z. Zhao, J. Li, Perovskite oxides: preparation, characterizations, and applications in heterogeneous catalysis, ACS Catal. 4 (2014) 2917–2940.

[35] O. Velle, A. Andersen, K.-J. Jens, The oxidative dehydrogenation of ethane by perovskite type catalysts containing oxides of strontium, cerium and ytterbium, Catal. Today 6 (1990) 567–574.
[36] C. Binet, M. Daturi, J.-C. Lavalley, IR study of polycrystalline ceria properties in oxidised and reduced states, Catal. Today 50 (1999) 207–225.
[37] Z. Wu, A.K.P. Mann, M. Li, S.H. Overbury, Spectroscopic investigation of surface-dependent acid–base property of ceria nanoshapes, J. Phys. Chem. C 119 (2015) 7340–7350.
[38] R.X. Valenzuela, G. Bueno, V.C. Corberán, Y. Xu, C. Chen, Selective oxidehydrogenation of ethane with CO_2 over CeO_2-based catalysts, Catal. Today 61 (2000) 43–48.
[39] C.T. Au, K.D. Chen, H.X. Dai, Y.W. Liu, C. Ng, The modification of Ho_2O_3 with $BaCl_2$ for the oxidative dehydrogenation of ethane, Appl. Catal. A Gen. 177 (1991) 185–191.
[40] A. Litke, Y. Su, I. Tranca, T. Weber, E.J.M. Hensen, J.P. Hofmann, Role of adsorbed water on charge carrier dynamics in photoexcited TiO_2, J. Phys. Chem. C Nanomater Interfaces 121 (2017) 7514–7524.
[41] Q. Du, R. Superfine, E. Freysz, Y.R. Shen, Vibrational spectroscopy of water at the vapor/water interface, Phys. Rev. Lett. 70 (1993) 2313–2316.
[42] J. Cao, Y. Ji, Z. Shao, Perovskites for protonic ceramic fuel cells: a review, Energy Environ. Sci. 15 (2022) 2200–2232.
[43] C. Yang, A. Grimaud, Factors controlling the redox activity of oxygen in perovskites: from theory to application for catalytic reactions, Catalysts 7 (2017).
[44] B.F. Serodio Costa, B.I. Arias-Serrano, A.A. Yaremchenko, Development of Ni-Sr(V, Ti)$O_{3-\delta}$ Fuel Electrodes for Solid Oxide Fuel Cells, Materials 15 (2021) 278.
[45] T. Noh, J. Kim, Y. Kim, H.H. Chun, M.-S. Jeon, H. Lee, Mn valence state and electrode performance of perovskite-type cathode $La_{0.8}Sr_{0.2}Mn_{1-x}Cu_xO_{3-\delta}$ (x=0, 0.2) for intermediate-temperature solid oxide fuel cells, Bull. Mater. Sci. 36 (2013) 1261–1266.
[46] Y. Feng, J. Luo, K.T. Chuang, Propane dehydrogenation in a proton-conducting fuel cell, J. Phys. Chem. C 112 (2008) 9943–9949.
[47] M.A. Chaar, D. Patel, H.H. Kung, Selective oxidation dehydrogenation of propane over V-Mg-O catalysts, J. Catal. 109 (1988) 463–467.
[48] E. Hernández, F. Baiutti, A. Morata, M. Torrell, A. Tarancón, Infiltrated mesoporous oxygen electrodes for high temperature co-electrolysis of H_2O and CO_2 in solid oxide electrolysis cells, J. Mater. Chem. A 6 (2018) 9699–9707.